Toward Reproducible Tract-specific In Vivo Diffusion Quantification in Human Cervical Spinal Cord

J. Xu[1], E. C. Klawiter[1], J. S. Shimony[2], A. Z. Snyder[1,2], R. T. Naismith[1], A. Priatna[3], T. Benzinger[2], A. Cross[1], and S-K. Song[2]
[1]Neurology, Washington University in St. Louis, St. Louis, MO, United States, [2]Radiology, Washington University in St. Louis, St. Louis, MO, United States, [3]Siemens Medical Solution, United States

Introduction High resolution *in vivo* axial human spinal cord diffusion tensor imaging (DTI) utilizing various reduced field-of-view (rFOV) techniques [1-6] has been recently reported. However, reproducibility of tract specific diffusion quantification is still hampered by small cross-sectional size, motion, and poor signal-to-noise ratio (SNR) [7]. We describe a comprehensive approach to improve the reliability of spinal cord DTI for longitudinal studies.

Methods Image Acquisition: MR images were acquired using either a 4-element (custom-fabricated) or a 3-element (neck posterior, vendor supplied) phased array coil on a 3 T scanner (Trio, Siemens). A previously described rFOV ss-SE-EPI sequence for optic nerve diffusion imaging [8] was further optimized with gradient moment nulling in the slice-selective (SS) direction (Fig. 1A). The slice-selective gradients for the excitation pulse were velocity-compensated and the spoiler gradients straddling the two refocusing pulses were removed in the SS direction. Images were acquired transaxially (FOV 72 × 28.8 mm, matrix 80 × 32, resolution 0.9 × 0.9 mm, TR/TE ~ 5000/99 ms, and slice thickness 5 mm) on 3 separate slice groups (C1-2, C3-4, and C5-6), each consisting of 6 slices. Landmarks in slice positioning are crucial in longitudinal studies, because of the thick slices and lack of anatomical markers in rFOV images. The center of the last slice of C2 was aligned with the end of the 2nd vertebra, while the center of the 2nd and 3rd slice group were aligned with the intervertebral discs between the adjacent vertebra (Fig. 1B white arrows). This arrangement accommodated the natural curvature of the human spine and enabled compensating for positioning differences in the same subject on different visits. Furthermore, slices were individually tiltable within the slice group to be parallel to the cross-section of the cord. Shimming volume was restricted to the spinal cord in both sagittal and coronal view (Fig. 1B and C). After automatic field-map based shimming, the line width was further optimized (FWHM < 45 Hz) by interactive adjustment. Each slice acquisition started with ~250-300 ms delay [9] after the rise of the sphygmic wave as measured with a peripheral pulse oximeter. Twenty-five diffusion weighted (DW) images with b values between 400-800 (b_{mean} = 600) s/mm^2 and randomly distributed diffusion encoding directions were acquired in addition to two b_0 images. Four repetitions including balanced acquisitions with opposite gradient polarity were averaged to increase SNR. For comparison, the minimal six directional DTI with a single shell of b = 600 s/mm^2 was also acquired in addition to one b_0 image. Sixteen repetitions, eight with opposite gradient polarity, were averaged to provide comparable SNR. The acquisition time of each slice group was ~ 8-10 min.

Data Analysis: A 3D affine registration restricted to translation was used for motion correction. An iterative approach was used to first align DW images to the preceding b_0 image, then the interspersed b_0 images were aligned to the first b_0 image and between averages. After registration, individual DW images were compared among averages and among adjacent slices in the same acquisition cycle. Outliers with abnormal distortion and signal dropouts, possibly due to arrhythmia, swallowing, or respiration, were removed and the remaining DW volumes were concatenated into the DWI dataset. The final preprocessing output was resampled resulting in voxels of 0.45 × 0.45 × 5 mm^3 before DTI calculation. DTI fitting using the conventional linear least-square (LLS) was compared to a non-linear Levenberg-Marquardt algorithm (NLLM) with novel non-negative Bayesian prior. The region-of-interests (ROI) for the posterior columns and lateral corticospinal tracts were determined based on the geometry of the cord. A long axis and short axis intersecting the central canal of the spinal cord were plotted as determined from the fractional anisotropy (FA) color map and b_0 image. The posterior spinal cord was further divided into four quadrants. A line joining the midpoints of the boundaries of the two lateral quadrants excluded central gray matter regions. ROIs of spinal cord tracts were defined in the remaining areas by excluding 1-2 layers of edge voxels (Fig. 2).

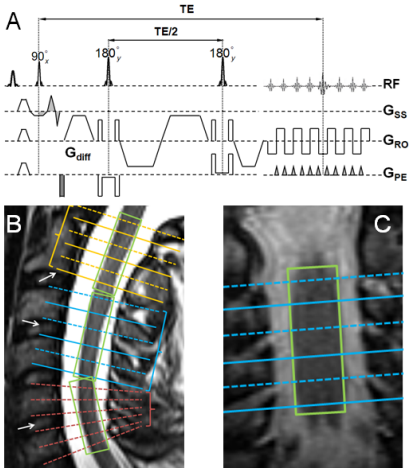

Figure 1. (A) Diffusion sequence scheme with gradient nulling in the SS direction. (B) Slice position with separate slice groups and tiltable slices within the group. White arrows are landmarks for slice positioning. Green boxes are the shimming volume. (C) Slice position and shimming volume in the coronal view.

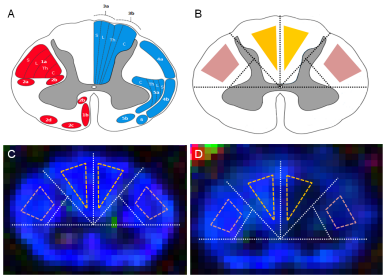

Figure 2. Anatomical reference (A) and proposed tract specific ROI methods based on geometry (B). FA color maps of a representative slice from C4 of a healthy subject (C) and a representative slice from C3 of a NMO patient (D) with lesions in the left corticospinal tract and posterior column.

Results and Discussion Motion was most prevalent in slices in C5-6, with increasing motion as the imaging proceeded caudally [10-11], probably attributable to respiration. Eddy-current induced distortion between b_0 and DW images and in-plane rotation were minimal. The effects of even mild motion (~2–3 mm, Fig. 3A) and corrupted DW images (12% outliers, Fig3. C) are significant for tract specific diffusion quantification. The six-direction DTI scheme usually yielded negative eigenvalues [11] in highly anisotropic structures, resulting in unity FA value (Fig. 4, orange arrows). The NLLM could not correct the misfit in constrained parameter searching space given the SNR challenge in spinal cord diffusion imaging. The randomized multi-b-shell 25-direction scheme provided not only enough redundancy for outlier rejection, but also greater searching space for the NLLM algorithm to correct negative eigenvalues (Fig. 4C, orange and red arrows). The lack of T1 or T2 contrast [12] between spinal cord GM and WM makes tract identification difficult, especially with coexistent pathology [13]. Tract specific ROI definition based on tractography [14-16] or fuzzy-logic classification [17] is inherently biased by diffusion measure. The geometry based ROI here provides an objective basis for unbiased quantification with limited number of voxels. Repeated scans of two subjects within a group of volunteers (n = 17) [18] showed an intraclass correlation coefficient (ICC) of directional diffusivity ($\lambda_{\parallel}$ and $\lambda_{\perp}$) < 15% for C2-5 and < 25% for C1 and C6. The comprehensive approach elaborated here shows promise for applying spinal cord DTI in longitudinal studies to detect Wallerian degeneration.

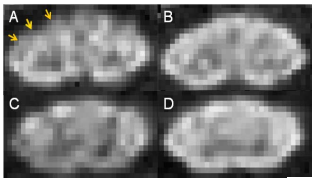

Figure 3. FA maps of a slice from C5 of a healthy subject without (A) and with (B) motion correction; and slice from C6 of a stable MS patient with good recovery without (C) and with (D) outlier rejection.

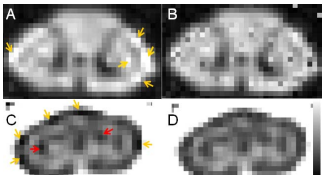

Figure 4. FA maps of a slice from C3 of a healthy subject by LLS (A) and NLLM (B) DTI fitting from the six-direction scheme. The smallest eigenvalue maps (scale bar: -0.2 – 1 μm^2/ms) of a slice from C6 of a healthy subject by LLS (C) and NLLM (D) DTI fitting from the randomized multi-b-shell 25-direction scheme.

Reference [1] Wheeler-Kingshott, et al. *NeuroImage* **16**: 93-102, 2002 [2] Jeong, et al. *Magn. Reson. Med.* **56**:1173-81, 2006 [3] Saritas, et al. *Magn. Reson. Med.* **60**: 468-73, 2008 [4] Wilm, et al. *Magn. Reson. Med.* **57**: 625-30, 2007 [5] Dowell, et al. *J. Magn. Reson. Imag.* **29**: 454-60, 2009 [6] Finsterbusch, *J. Magn. Reson. Imag.* **29**: 987-93, 2009 [7] Barker, *J. Neurol. Sci.* **186**: S45-9, 2001 [8] Xu, et al. *NMR Biomed*. **21**: 928-40, 2008 [9] Summers, et al. *Am. J. Neuroradiol*. **27**: 1952-61, 2006 [10] Kharbanda, et al. *Magn. Reson. Med.* **56**: 334-339, 2006 [11] Santarelli, et al. *Magn. Reson. Imag.* in press, 2009 [12] Smith, et al. *Magn. Reson. Med.* **60**: 213-9, 2008 [13] Farrell, et al. *Magn. Reson. Med.* **59**: 1079-89, 2008. [14] Figley and Stroman, *Magn. Reson. Med.* **58**: 185-189, 2007 [15] Cirrarelli, et al. *Brain* **130**: 2220-31 2007 [16] Hecke, et al. *J. Magn. Reson. Imag.* **27**: 978-91 [17] Ellingson, et al. *Ann. Biomed. Eng.* **36**: 224-36, 2007 [18] Xu, et al. *Proc. ISMRM*, **17**: 3224, 2009